HHS Public Access

Author manuscript

Nat Neurosci. Author manuscript; available in PMC 2017 October 24.

Published in final edited form as:

Nat Neurosci. 2017 June ; 20(6): 854–863. doi:10.1038/nn.4554.

Delay Activity of Specific Prefrontal Interneuron Subtypes Modulates Memory-Guided Behavior

Tsukasa Kamigaki and **Yang Dan***

Division of Neurobiology, Department of Molecular and Cell Biology, Helen Wills Neuroscience Institute, Howard Hughes Medical Institute, University of California, Berkeley, CA 94720

Abstract

Memory-guided behavior requires maintenance of task-relevant information without sensory input, but the underlying circuit mechanism remains unclear. Calcium imaging in mice performing a delayed Go/No-Go task revealed robust delay activity in dorsomedial prefrontal cortex (dmPFC), with different pyramidal neurons signaling Go and No-Go action plans. Inhibiting pyramidal neurons by optogenetically activating somatostatin (SST)- or parvalbumin (PV)-positive interneurons, even transiently during an early delay period, impaired task performance primarily by increasing inappropriate Go responses. In contrast, activating vasoactive intestinal peptide (VIP)-positive interneurons enhanced the behavioral performance and neuronal representation of action plans. Furthermore, while the natural activity of SST and PV neurons was strongly biased toward Go trials, VIP neurons were similarly active in Go and No-Go trials. SST/VIP neuron activation also impaired/enhanced performance of a delayed two-alternative forced choice task. Thus, dmPFC is a crucial component of the short-term memory network, and activation of its VIP neurons improves memory retention.

INTRODUCTION

The prefrontal cortex (PFC) is known to play a key role in active maintenance of task-relevant information for memory-guided behavior[1–3]. In primates performing tasks that involve a delay between the visual cue and the motor response (delayed-response tasks), lesion or inactivation of the dorsolateral PFC strongly disrupts the task performance, with severity of the impairment increasing with the length of the delay[2,4–6]. In contrast, when the visual cue is presented continuously to guide the behavior (visually-guided tasks), the performance remains largely intact. This indicates that the impairment induced by PFC

*Correspondence to: ydan@berkeley.edu.

Data and code availability

The data that support the findings of this study are available from the corresponding author upon reasonable request. MATLAB codes can be requested from the corresponding author.

Author Contributions

T.K. performed all the experiments and analyzed the data. T.K. and Y.D. conceived and designed the experiments and wrote the manuscript.

Competing Financial Interests

The authors declare no competing financial interests.

lesion or inactivation is specific for memory maintenance. Recent studies have shown that inactivation of the PFC in rodents causes similar memory impairments[7–12].

Consistent with these lesion and inactivation studies, electrophysiological recordings have shown that many PFC neurons exhibit sustained activity during the delay period, which carries task-relevant information[7,9–11,13–20]. However, the causal relation between the delay-period activity and short-term memory maintenance is only beginning to be examined, as disruption of activity specifically during the delay without affecting other task periods requires a high temporal precision, which is afforded by the optogenetic approach[8–12,20]. Furthermore, while dynamical systems models of these optogenetic data[8,11] support the theory that attractor networks may sustain the delay activity without sensory input, many questions remain about the roles of different neuronal subtypes in implementing these networks. In particular, the neocortex contains a diversity of GABAergic interneurons, which play key roles in cortical computation. Different subtypes of interneurons are differentially modulated by sensory stimuli, motor behaviors, and neuromodulatory inputs, and they play distinct roles in shaping pyramidal neuron activity[21–29]. Characterizing the functional role of each cell type is a critical step in understanding the circuit mechanism of working memory maintenance.

In this study, we used cell-type-specific calcium imaging to measure the delay-period activity of pyramidal neurons and three major interneuron subtypes in the PFC of mice performing a delayed-response task. Bidirectional optogenetic manipulations were used to test their causal roles in memory maintenance. We found that suppression of pyramidal neuron activity through activation of somatostatin (SST)- or parvalbumin (PV)-positive interneurons, even transiently during an early delay period, severely impaired task performance. In contrast, activation of vasoactive intestinal peptide (VIP)-positive interneurons enhanced both the neuronal coding of action plans and task performance of the animal. Furthermore, the endogenous delay activity of SST and PV neurons is strongly biased toward Go trials, whereas VIP neurons are similarly active in Go and No-Go trials. Our results reveal the functional distinction among three interneuron subtypes in working memory maintenance, and they point to the potential for improving memory performance by activating VIP interneurons in the PFC.

RESULTS

Delay activity of different pyramidal neurons signals Go and No-Go action plans

To examine the function and mechanism of delay-period activity in the PFC, we trained head-fixed mice on a delayed Go/No-Go auditory discrimination task (Fig. 1a and Supplementary Video 1, Methods). Each trial consists of sample, delay, and test periods. During the sample period (2 s) a target (8 kHz) or non-target (2 kHz) auditory stimulus was presented (the corresponding trial was referred to as a “Go” or “No-Go” trial, respectively), followed by a 5 s delay period during which water was inaccessible. The test period began when the water port was presented; licking in Go trials within the 2 s response window (Hit) was rewarded, and licking in No-Go trials (False Alarm) was punished. Mice learned this task within several weeks, licking mostly during the test period (Fig. 1a and Supplementary Fig. 1), and their correct response rate stabilized at 84 ± 2.6 % (s.e.m., n = 9 mice, Fig. 1b).

Pupillometry during the task suggests similar levels of arousal during Go and No-Go trials (Supplementary Fig. 2). However, the great majority of errors were False Alarms (Fig. 1c), indicating that the task performance depends mainly on the successful suppression of inappropriate Go responses.

To image task-related neuronal activity, we injected Cre-inducible adeno-associated virus (AAV) expressing the calcium indicator GCaMP6f[30] into the dmPFC of CaMKIIα-Cre mice for specific labeling of pyramidal neurons[27]. Imaging was performed through a gradient refractive index (GRIN) lens coupled to a miniaturized integrated fluorescence microscope[31], which allows monitoring of neuronal activity across cortical layers (Fig. 2a).

We found strong task-related activity in dmPFC pyramidal neurons. In addition to the calcium transients time-locked to the sensory stimuli and trial outcomes[27], many neurons exhibited sustained activity during the 5-s delay period (Fig. 2b–h). While some neurons were selectively activated in Go trials (referred to as significant “Go-preferring neurons”; Fig. 2b,d,f,h), others were much more active in No-Go trials (significant “NG-preferring neurons”; Fig. 2c,e,g,h), similar to a previous observation in mouse M1[32]. Interestingly, we found a higher fraction of NG-preferring neurons in deeper cortical layers (Fig. 2i, see Supplementary Fig. 3 for analyses at different dorsal-ventral positions), suggesting a transformation of action plan representation across cortical layers[10]. To quantify the separability between the two action plans encoded in dmPFC activity, we computed the Euclidean distance between the population activity in Go and No-Go trials (Methods). The distance increased rapidly after the onset of auditory stimulus and persisted throughout the delay and test periods (Fig. 2j). Decoding analysis also showed that the delay activity in individual trials was highly predictive of the motor behavior in correct response (Hit and Correct Rejection) trials (Supplementary Fig. 4), indicating that information on the action plan was maintained in dmPFC activity.

Delay activity of pyramidal neurons is required for memory maintenance

Previous studies showed that the encoding of future actions in PFC activity improves with behavioral learning in both rats[18] and monkeys[33]. Here, the Euclidean distance between the Go and No-Go delay activity was also positively correlated with the task performance (Fig. 2k; $R = 0.50$, $P = 0.0081$, Pearson’s correlation coefficient, bootstrap), suggesting a functional contribution of this activity in behavioral control. To test directly the causal relationship between dmPFC activity and memory maintenance, we suppressed pyramidal neuron spiking by optogenetically activating inhibitory interneurons[9–12,20] (Supplementary Fig. 5). Multielectrode recordings showed that channelrhodopsin-2 (ChR2)-mediated SST neuron activation strongly suppressed dmPFC spiking in both Go and No-Go trials (Supplementary Figs. 5, 6, 7a), leading to a marked reduction in their Euclidean distance (Supplementary Fig. 7b). Previous studies showed that activation of PV neurons is also highly effective in suppressing pyramidal neuron activity[9–11,29]. Behaviorally, activation of either SST or PV neurons caused a strong impairment in task performance, with a substantial increase in False-Alarm rate and a small decrease in Hit rate (Fig. 3a–c). Thus, dmPFC pyramidal neuron activity is important for the delayed response task, especially for the suppression of inappropriate motor responses in No-Go trials.

Suppression of dmPFC activity during the whole trial could affect encoding of the auditory stimulus, retention of the action plan, and/or execution of the motor response. To test specifically the role of dmPFC activity in memory retention, we applied optogenetic suppression briefly within the delay period[8–12,20]. Strikingly, even a 2-s laser stimulation of SST or PV neurons during early delay caused a strong reduction in behavioral performance (Fig. 3d–f), indicating that the delay activity plays a crucial role in maintaining the Go/No-Go action plan after cessation of the auditory stimulus. In contrast, activating SST or PV neurons in the primary somatosensory cortex, during either the whole trial or early delay period, had no significant effect on performance (Supplementary Fig. 8), indicating that the behavioral impairment was not a general side effect of laser stimulation.

VIP neuron activation improves task performance and neural coding of action plans

Unlike SST or PV neuron activation, which powerfully suppresses pyramidal neuron activity (Supplementary Fig. 7a), VIP neuron activation causes both inhibition and disinhibition of pyramidal neurons[22,25,26,34]. We next tested their role in memory-guided behavior. Optogenetic activation of VIP interneurons in dmPFC – either throughout the whole trial or only during the early delay period – caused a marked improvement in task performance (Fig. 4a,b). Conversely, archaerhodopsin (Arch)-mediated silencing of VIP neurons caused a significant behavioral impairment (Fig. 5a,d), indicating that their normal activity is important for performing the task. Both the ChR2-mediated increase and Arch-mediated decrease in correct response rate were due primarily to changes in False-Alarm rate (Fig. 4a,b and 5a,d). This suggests that the main effect of VIP neuron activation is to improve the suppression of inappropriate Go responses, opposite to the effect of SST or PV neuron activation (Fig. 3). In control experiments in the primary somatosensory cortex, VIP neuron manipulation caused no significant change in performance (Supplementary Figs. 9, 10), indicating a specific role of the dmPFC.

Previous studies have shown that VIP neuron activation disinhibits pyramidal neurons by inhibiting SST and PV interneurons[25,26,34,35]. Arch-mediated optogenetic inhibition of SST or PV neurons, either throughout the whole trial or during the early delay period, significantly improved task performance (Fig. 5b,c,e,f), suggesting that the behavioral effect of VIP neuron activation could indeed be mediated in part by inhibiting SST and PV neurons. On the other hand, direct optogenetic activation of dmPFC pyramidal neurons impaired behavioral performance (Supplementary Fig. 11), indicating that a non-selective increase in their firing rate is detrimental.

To further examine the mechanism by which VIP neuron activation improves the behavior, we performed multielectrode recordings in the dmPFC (Fig. 6a). For the recorded Go-preferring neurons, laser stimulation significantly decreased their delay activity in No-Go trials ($P = 0.00055$, paired t-test) but not in Go trials ($P = 0.18$) (Supplementary Fig. 12), resulting in an increased difference between their Go and No-Go activity (Fig. 6b, left). For the NG-preferring neurons, laser decreased the activity in Go trials ($P = 0.034$) but not in No-Go trials ($P = 0.58$), leading to a decreased Go – NG value (Fig. 6b, right). For the remaining unmodulated neurons, the activity decreased in both Go ($P < 0.001$) and No-Go trials ($P < 0.001$). Thus, while VIP neuron activation caused an overall decrease in dmPFC

activity, the magnitude of the effect depended on both the trial type (Go vs. No-Go) and the functional property of the cell. Such differential modulations resulted in an increased Euclidean distance between Go and No-Go delay-period activity (Fig. 6c), which may contribute to the improved behavioral performance (Fig. 2k).

Natural delay-period activity of SST, PV, and VIP interneurons

Having demonstrated their distinct impacts on memory retention using optogenetic manipulations, we next measured the natural task-related activity of the interneuron subtypes to assess their physiological contributions to memory-guided behavior. Cre-inducible AAV expressing GCaMP6f was injected into the dmPFC of SST-, PV-, or VIP-Cre mice, and calcium imaging was performed during the delayed response task (Fig. 7a–c).

While the activity of SST and PV neurons was biased strongly toward Go trials (Fig. 7a,b), the VIP neuron population showed similar activity in Go and No-Go trials (Fig. 7c). Among the three interneuron subtypes and pyramidal neurons, VIP neurons exhibited the highest relative activity in No-Go trials (Fig. 7d, $P < 0.001$ for all comparisons, Tukey-Kramer post-hoc test following one-way ANOVA). Since optogenetic activation and inactivation of VIP neurons in No-Go trials improved and impaired the suppression of inappropriate motor responses, respectively (Fig. 4 and Fig. 5a, d), the natural activity of VIP neurons in these trials may play an important role in enabling high performance of the delayed Go/No-Go task.

Interneuron activation during delayed two-alternative forced choice task

Performance of the delayed Go/No-Go task depends mainly on the successful suppression of inappropriate Go responses (Fig. 1c), and the effects of interneuron manipulations reported above were due primarily to changes in the False-Alarm rate (Figs. 3–5). These observations point to a crucial role of the dmPFC in response inhibition[2,3,36]. However, even transient optogenetic manipulations during an early delay period significantly affected the performance (Figs. 3d,e,f, 4b, 5d,e,f), arguing against a simple effect on motor suppression during the response period (although it is possible that some ChR2- and Arch/Halo-mediated changes in cortical activity outlast the laser stimulation by several seconds). In addition to changes in the False-Alarm rate, several manipulations also had small but significant effects on Hit rate (Figs. 3b,e, 4a,b), which cannot be accounted for by a pure response inhibition.

To further examine the roles of dmPFC SST and VIP interneurons in memory-guide behavior separately from response inhibition, we trained mice to perform a delayed two-alternative forced choice (2-AFC) task, in which they licked either the left or right water port in response to a tone stimulus after a variable delay period (1.5–2 s) (Fig. 8a). We found that ChR2-mediated bilateral activation of SST neurons, during either the whole trial or an early delay period, significantly impaired the behavioral performance, whereas VIP neuron activation improved the behavior (Fig. 8b–e), consistent with the findings using the delayed Go/No-Go task (Figs. 3–4). These results further demonstrate the functions of the dmPFC interneurons in memory-guided behavior beyond response suppression.

DISCUSSION

Using a combination of calcium imaging and bidirectional optogenetic manipulations during memory-guided behavior, we have revealed distinct functional roles of three major subtypes of dmPFC GABAergic interneurons in short-term memory maintenance. While activation of SST and PV interneurons impairs behavioral performance by suppressing the delay-period activity of pyramidal neurons, activation of VIP interneurons improves their representation of the action plans and task performance of the animal. These results indicate that the dmPFC is a crucial component of the short-term memory network, and activity of its VIP neurons plays a key role in memory retention.

The strong behavioral impairment caused by a transient dmPFC inactivation in well trained mice (Fig. 3) is reminiscent of the finding in rat frontal orienting field (FOF)[8], and it suggests a crucial role of the delay activity in maintaining memory for the action plan[37–39]. However, the rat FOF neuronal activity in error trials reflects the motor responses better than the instructing sensory stimuli[7], whereas the mouse dmPFC activity in False-Alarm trials was more similar to that in Correct-Rejection trials than in Hit trials (Fig. 2d–g, Supplementary Fig. 4). The difference between these observations could be due to the difference in the brain region studied or to the difference in task design (2-AFC vs. Go/No-Go). Unlike the 2-AFC task that involves symmetric left and right motor responses, Go/No-Go tasks are intrinsically asymmetric, with far more False-Alarm than Miss errors (Fig. 1c). It is thus possible that when the animal is motivated to lick, even a slight deviation of dmPFC activity from the pattern required for Correct Rejection could lead to an inappropriate Go response. The Miss errors, on the other hand, increased dramatically near the end of each behavioral session (likely due to water satiety), suggesting that a significant fraction of them are related to lower levels of motivation. A full understanding of how dmPFC activity is decoded during this behavior will require observing neuronal activity in the downstream circuits. Our finding is also different from a recent study using a delayed non-match to sample task, in which the delay activity of a more ventral region of the medial PFC was found to be important for learning of the task, but not for its performance after the mice were well trained[20]. In addition to the differences in brain region (ventral vs. dorsal mPFC) and sensory modality (olfactory vs. auditory), there is an important difference in the memory requirement for the two tasks. While the delayed non-match to sample task requires short-term memory of the sensory cue, the delayed-response task is likely to require maintenance of the action plan.

Besides the frontal cortex, delay-period activity has also been observed in other brain regions including the parietal cortex, the superior colliculus, and the temporal lobe[8,40–43]. These regions are anatomically connected to the PFC[44], and during working-memory tasks their activity is often synchronized with PFC activity, with the strength of synchronization predictive of the animals' performance[42,45,46]. Such inter-areal interactions are likely to be important for the maintenance of delay-period activity without sensory input, although the relative importance of the different regions in various memory-guided tasks remains to be investigated.

Consistent with previous studies based on muscimol inactivation[32,47], our manipulations of mouse dmPFC activity strongly affected the False-Alarm rate (Fig. 3 and Fig. 4), indicating a key role of this circuit in suppressing inappropriate motor responses. NG-preferring pyramidal neurons were found to be much more abundant in deep cortical layers (Fig. 2i), raising the possibility that these cells project to distinct downstream targets[48]. One potential target is the subthalamic nucleus, which is selectively activated when subjects inhibit their motor responses, and this activity is correlated with PFC activity[36,49]. Other targets of the PFC include neuromodulatory circuits such as the dorsal raphe nucleus, which contains serotonergic neurons that are important for impulse control. A recent study showed that optogenetic activation of dorsal raphe serotonergic neurons in the mouse suppresses premature responding[50]. Notably, these serotonergic neurons also project to the PFC and can activate its VIP neurons through ionotropic serotonin receptors[25]. Such reciprocal interactions between the PFC and the dorsal raphe nucleus may boost the signals in both circuits for impulse suppression.

We found that SST neuron activation caused a stronger behavioral impairment than PV neuron activation (Fig. 3), consistent with a recent study using a delayed non-match-to-place behavioral paradigm[12]. The SST neurons also exhibited stronger Go-preferring delay activity than PV neurons (Fig. 7), which may be related to their observation that SST cells show stronger target-dependent delay activity. The most striking difference observed in our study, however, is between VIP and SST/PV interneurons. Although VIP neuron activation caused an overall decrease in dmPFC activity, the magnitude of the effect depended on both the functional property of the cell (Go- vs. NG-preferring) and the trial type (Go vs. No-Go, Fig. 6b, Supplementary Fig. 12), leading to an increased Euclidean distance between the Go and No-Go trials (Fig. 6c). The overall decrease in activity could be mediated by direct inhibition of pyramidal neurons by VIP interneurons[25,26,35], whereas the context-dependent firing rate modulation could be partly mediated by disinhibition of pyramidal neurons through suppression of SST or PV neurons[22,25,26,34,35]. Interestingly, while optogenetic stimulation of pyramidal neurons impaired the task performance (Supplementary Fig. 11), presumably because the indiscriminate activation of Go- and NG-preferring neurons disrupted the specific activity patterns important for behavioral control, activating the VIP neuron population improved the performance (Fig. 4). This suggests that the overall level of VIP neuron activity, which is likely regulated by the degrees of arousal and task engagement, plays a key role in modulating the behavioral performance. VIP neurons receive numerous glutamatergic inputs from other cortical areas[25,34] and neuromodulatory inputs from subcortical regions[22]. Thus, these interneurons may serve as a point of convergence for multiple inputs to regulate memory maintenance by the prefrontal cortex.

Online Methods

Animals

All experimental procedures were approved by the Animal Care and Use Committee at the University of California, Berkeley. Calcium imaging experiments were performed in CaMKIIα-Cre (Jackson lab stock 005359)[51], PV-Cre (008069), SST-Cre (013044) and VIP-Cre (010908) mice. For optogenetic activation and electrophysiology experiments in the

delayed Go/No-Go task, SST-Cre, PV-Cre or VIP-Cre mice were crossed with loxP-flanked-ChR2-eYFP mice (012569). For pyramidal cell activation, wild type mice (C57) injected with AAV2/2-CaMKIIα-hChR2(H134R)-EYFP were used. Optogenetic inactivation experiments were performed using PV-Cre, SST-Cre, VIP-Cre mice injected with AAV2-CAG-FLEX-ArchT-tdTomato, and PV-Halo mice (PV-Cre mice crossed with loxP-flanked-Halo-EYFP mice (014539)). Optogenetic activation experiments in the delayed 2-AFC task were performed using SST-Cre or VIP-Cre mice injected with AAV2-EF1α-FLEX-ChR2–eYFP. Animals were housed on a 12-h dark/12-h light cycle (light on between 7:00 and 19:00). All the experiments were carried out between 8:00 and 17:00. Imaging, optogenetic, and electrophysiology experiments were performed on adult mice (2–8 months old, including both genders, singly housed, and naive before experiments). Data collection and analysis were not performed blindly.

Surgery

Adult mice (2–8 months old) were anesthetized with isofluorane (3% induction and 1.5% maintenance) and placed on a stereotaxic frame (David Kopf Instruments). Temperature was kept stable throughout the procedure using a heating pad. The mice received buprenorphine (0.05 mg/kg) and supplementary analgesia (meloxicam, 10 mg/kg).

For imaging experiments, animals underwent the following surgical procedures. First a craniotomy of ~500 μm was made to target the dmPFC (AP +1.8–2.1 mm, ML 0.3–0.5 mm, DV 0.8–1.0 mm from bregma), where we injected 600–800 nL of AAV1-flex-GCaMP6f (Penn Vector Core) through a borosilicate pipette using a microinjector (Nanoject, Drummond Scientific). A stainless steel headplate was then affixed to the skull using machine screws and dental cement mixed with carbon powder (Sigma) to make it opaque. After a week of recovery, the mice underwent the initial stages of behavioral training (habituation and conditioning) for approximately 2 weeks. We then performed a second surgical procedure to implant the gradient refractive index (GRIN) lens (Inscopix, diameter: 1 mm; length: 4.2 mm; pitch: 0.5; numerical aperture: 0.5) to target the dmPFC (center: AP +1.8–2.1 mm, ML 0.3–0.5 mm). We expanded the virus-injection craniotomy to ~1 mm and slowly aspirated the superficial tissue using a blunt 27G needle connected to a vacuum pump, avoiding blood clotting by constantly irrigating the tissue with sterile Ringer's solution. After ensuring there was no active bleeding, the GRIN lens was gently placed upon the tissue and the space between the lens and the skull was filled with 1.5% agar. The lens was then cemented to the rest of the implant and covered with a plastic cap. The mice recovered from this procedure for at least 3 days and water restriction was reinstated for training. Once the mice reached criterion performance (see "Behavioral procedure" below), we implanted the baseplate for chronic imaging[52]. Since this was not an invasive procedure, the mice were head-fixed and lightly anesthetized with 0.5–1% isofluorane. The protective plastic cap was removed to expose the surface of the lens and the miniature microscope attached to the baseplate was lowered with a micromanipulator to the desired focal plane. The baseplate was then cemented to the rest of the implant, and covered with a protective cap after the microscope had been retracted.

For optogenetic activation experiments in the delayed Go/No-Go task, we implanted a stainless steel headplate for head fixation and guide cannulas (22G, Plastics One) at the surface above the right dmPFC (AP +1.8–2.1 mm, ML 0.3–0.4 mm, DV 0 mm) and above the right vibrissa primary sensory cortex, vS1 (AP −1.5 mm, ML 3.5 mm, DV 0 mm) in VIP-ChR2, SST-ChR2, or PV-ChR2 mice. For optogenetic activation experiments in the delayed 2-AFC task, we injected AAV for ChR2 (AAV2-EF1α-FLEX-ChR2–eYFP, University of North Carolina Vector Core, 600–800 nL) in the dmPFC bilaterally (AP +1.8–2.1 mm, ML 0.3–0.4 mm, DV 0.8–1.2 mm) in VIP-Cre, or SST-Cre mice.

For optogenetic inactivation experiments, we injected AAV for Arch (AAV2-CAG-FLEX-ArchT-tdTomato, University of North Carolina Vector Core, 600–800 nL) in the dmPFC (AP +1.8–2.1 mm, ML 0.3–0.4 mm, DV 0.8–1.0 mm) and in the vS1 (AP -1.5 mm, ML 3.5 mm, DV 0.8 mm) in VIP-Cre, SST-Cre, or PV-Cre mice. After a week of recovery, we implanted a headplate with a guide cannula at the same coordinates as in optogenetic activation experiments to target the dmPFC and the vS1.

Histology

We performed histology to confirm the location of the implanted GRIN lens in imaging experiments, the cannulas used in optical stimulation experiments, and the recording sites in electrophysiology experiments. At the end of the experiments, the mice were deeply anesthetized with isoflurane and immediately perfused with chilled 0.1 M PBS followed by 4% paraformaldehyde (wt/vol) in PBS. The brain was removed and post-fixed overnight at 4 °C. After fixation, the brain was placed in 30% sucrose (wt/vol) in PBS solution for 1–2 days at 4 °C. After embedding and freezing, the brain was sectioned into 50 μm coronal slices using a cryostat (Thermo Fisher Scientific). The slides were mounted with VECTASHIELD® mounting medium with DAPI (Vector Laboratories) and examined with a Microphot-SA fluorescence microscope (Nikon Corp.).

Behavioral procedure

Delayed Go/No-Go auditory task—We trained head-fixed mice for a delayed Go/No-Go auditory task (Fig. 1a) using a customized code in the Presentation software (Neurobehavioral Systems). Behavioral training started with habituation (2–3 days), in which there was no auditory stimulus and the mouse was given free water rewards (~4 μL) for each lick. In the conditioning phase, the mouse was trained to lick in response to a target tone stimulus (8 kHz, 65 dB). Each trial started with a target tone for 2 s, followed by a water port presentation within reach of the tongue. If a lick was detected within the first 2 s after the water port presentation (response window), the mouse was rewarded with ~4 μL of water. If no lick was detected during the response window, water reward was given after the end of the response window during this conditioning phase. Once the number of licks exceeded 150 within 30 min, the mouse was advanced to the next phase. In the next discrimination phase, each trial had the same temporal structure, but the auditory stimulus was either the target or non-target (2 kHz, 65 dB) tone (Go or No-Go trials, respectively). The Go and No-Go trials were randomly interleaved, but the same auditory stimulus was never presented more than five consecutive times. Initially the temporal delay between the end of the auditory stimulus and the water port presentation was zero, and increased in 500-

ms step when behavioral performance reached ~70% correct in a 50-trial block. In this experiment, licks were detected by an infrared beam-break lickometer in order to monitor licking even during the delay period when the water port was retracted. Comparison with the licks detected from video recording showed that the infrared detector was highly reliable.

After behavioral performance with the 5 s delay reached ~70% correct for more than 3 consecutive days, we started the main experiments including calcium imaging, optogenetic, and electrophysiology experiments. If the mice failed to reach the criterion performance, they were not further used for the experiments. At the start of the trial, mice were presented with an auditory stimulus for 2 s (target or non-target tones, sample period). The sample period was followed by a 5 s delay period, and then a water port is presented (test period). Lick in response to a target tone within the first 2 s after the water port presentation (response window) was rewarded with a drop of water delivered through the water port (Hit), while lick to a non-target tone triggered a combination of airpuff to the cheek (15–20 psi, 200 ms), electric shock at the tip of the tongue (less than 1 mA), and 7 s timeout period (False Alarm, FA). Water reward was delivered immediately after the first lick during the response window in Hit trials. Inter-trial intervals was 7.5 s. No-lick to a target or non-target tone within the 2 s response window was regarded as Miss or Correct Rejection (CR), respectively. The water port was retracted after 2 s from the first lick during the response window in Hit and FA trials, or 2 s after the end of the response window in Miss and CR trials. Even though no water was delivered in No-Go (including CR and FA) trials, animals tended to lick the empty water port, which remained for 2 s after the response window (Fig. 1a). In some cases the mice continued to lick even after getting a shock, consistent with the general observation that in the Go/No-Go licking task resisting the temptation to lick is a major challenge for the mice.

Delayed two-alternative forced choice (2-AFC) task—Each trial consists of sample, delay, and test periods. During the sample period (2 s) an auditory stimulus (either 2 kHz or 8 kHz tone, 65 dB) was presented (the corresponding trial was referred to as a “Left” or “Right” trial, respectively), followed by a variable delay period (1.5 to 2 s) during which water was inaccessible. At the beginning of the test period, both the left and right water ports were simultaneously presented; lick left in Left trials within the 2 s response window was rewarded (Correct), and licking right was punished with a combination of airpuff to the cheek and a 7 s timeout period (Error); *vise versa* for Right trials. Inter-trial interval was 7.5 s. No lick within the 2 s response window was also regarded as Error, although no punishment was applied. The water port was retracted 2 s after the first lick during the response window in both Correct and Error trials. In this experiment, licks were detected by each of the two water ports via an electrically coupled circuit board.

Microendoscopic calcium imaging

The detailed procedure was described elsewhere[27]. Briefly, we performed cellular-resolution microendoscopic calcium imaging from genetically defined cell types in the right dmPFC using a miniaturized integrated fluorescence microscope (Inscopix; 20x objective; LED power: 0.2–0.7 mW; CMOS sensor resolution: 1,440 × 1,080 pixels) coupled to a GRIN lens[31]. Images were acquired at 20 frames/s using nVista HD (Inscopix). Behavioral events

were synchronized with imaging by acquiring analogue voltage output by both the imaging acquisition and behavioral control software using a custom code in LabVIEW (National Instruments).

Optogenetic stimulation

To activate or silence each cell type during the behavioral task, we applied blue laser (473 nm; CrystaLaser, step pulse, 5 mW at fiber tip) or yellow laser (593 nm; step pulse 15–20 mW at fiber tip) through an optic fiber (200 μm diameter) under the control of a stimulator (Grass). For optogenetic activation/inactivation experiments, an optic fiber mounted on a micromanipulator (Narishige) was inserted through the implanted guide cannula to target the dmPFC or the vS1 at the depth of 0–0.5 mm from the surface. For electrophysiology experiments, the optic fiber was placed < 1 mm from the recording site. For the delayed Go/No-Go task, in the whole trial condition, laser stimulation started with the presentation of an auditory stimulus and continued for 9.3 s, thus covering from the sample period to the end of the response window in each trial. In the early delay condition, laser stimulation started with the delay period onset and lasted for 2 s, thus covering the early portion of the delay period in each trial. For the delayed 2-AFC task, in the whole trial condition, laser stimulation started with the tone onset and continued for 6 s to cover from the sample period to the end of the response window in each trial. In the early delay condition, laser stimulation started with the delay period onset and lasted for 1 s, thus covering the early portion of the delay period in each trial. Laser stimulation was applied in 50% of pseudo-randomly selected trials, but the same condition never occurred in more than 5 consecutive trials.

Electrophysiology

For electrophysiology recording from behaving mice, the body of the mouse was placed in a metal tube (2.9 cm inner diameter) and the headplate was fixed on a holder. While the animal was under gas anaesthesia (1.5% isoflurane in oxygen), a craniotomy (~1 mm diameter) was made over the target area in the dmPFC (center AP +1.8–2.1 mm, ML 0.3–0.5 mm). A silicon probe (A1×16-Poly2-5mm-50s-177-A16, 16 active channels separated by 50 μm, NeuroNexus Technologies) was inserted using a motorized micromanipulator (MX7630R, Siskiyou). Signals were recorded with the Cheetah 32 channel acquisition system (Neuralynx), filtered at 0.6–6 kHz and sampled at 30 kHz. After every daily experiment, the craniotomy was sealed with a silicone elastomer (Kwik-Cast, World Precision Instruments). At the end of the experiment, a silicon probe coated with DiI was inserted to mark the recording tract. 5 VIP-ChR2 mice and 6 SST-ChR2 mice were used for these experiments.

Spike sorting

Spikes were sorted offline on the basis of the waveform energy and the first three principal components of a spike waveform (Supplementary Fig. 6). We grouped nearby channels of the silicon probe into groups of three and performed semiautomatic spike sorting using the software KlustaKwik (http://klustakwik.sourceforge.net). Spike clusters were considered single units if their auto-correlograms had a 2-ms refractory period and their cross-correlograms with other clusters did not have sharp peaks within 2 ms of 0 lag.

Pupillometry

We monitored the pupil during the delayed Go/No-Go task using an infrared camera placed approximately 2 cm away from the animal's eye. Images were acquired at a frame rate of 30 Hz. Each frame was converted to a binary image and the pupil was fitted with an ellipse to measure its diameter using custom-written software in MATLAB. For each session, pupil diameter was normalized by the mean value during the 3 s inter-trial interval period immediately preceding the sample period, averaged across all the Go and No-Go trials.

Imaging data analysis

Image processing was performed in the same way as previously described[27]. The acquired images were first spatially downsampled by a factor of 4. Image stacks were then corrected for lateral motion using an algorithm based on a previous study[52]. Regions of interest (ROIs) were drawn manually using a custom-written MATLAB program, based on visual inspection of the fluorescence signals recorded in each session; cells that showed at least one fluorescence transient in the session were selected. We also compared our method with a commonly used method based on pixel-wise activity map[27,53] and found that the ROIs corresponded closely to the activity map. To correct for potential contamination from out-of-focus neuropil fluorescence, for each ROI we subtracted from the raw fluorescence (F_{raw}) the average fluorescence over a 20-μm ring surrounding that ROI (F_{np}): $F_{subt}(t) = F_{raw}(t) - cf \times F_{np}(t)$, where cf is a correction factor estimated as the ratio between the average fluorescence over a blood vessel and the neuropil adjacent to that blood vessel, both subtracted by a DC offset given by the intensity of off-lens pixels. The obtained cf value was 0.77 ± 0.01 (mean ± s.e.m.), compatible with other reports that used similar methods[30,54]. To correct for decreases in baseline fluorescence due to bleaching of the calcium indicator we subtracted slow fluctuations in baseline according to the expression: $F_{corrected}(t) = F_{subt}(t) - G(t) + \langle F_{subt}(t) \rangle$, where brackets indicate time average over the entire recording session and $G(t)$ is the average of $F_{subt}(t)$ over a 300-s sliding window. Finally, average fluorescence for each ROI was calculated as $\Delta F/F(t) = (F_{corrected}(t) - \langle F \rangle)/\langle F \rangle$, where $\langle F \rangle$ is the average fluorescence across the entire recording. Unless otherwise stated, ΔF/F was z-scored using the fluorescence signal during the baseline period (1 s period immediately before the start of the sample period) for each trial type.

To assess whether a cell was significantly modulated by the task, we performed a one-way ANOVA with a factor of trial types (Hit or CR) for the delay activity. In each cell, z-scored ΔF/F was averaged over the delay period. A cell was defined as a significant "Go-preferring" cell if $P < 0.05$ with higher activity in Hit trials than CR trials, or as a significant "No-Go (NG)-preferring" cell if $P < 0.05$ with higher activity in CR trials. To further assess the task-related activity in Fig. 2d–g and Fig. 7a–c, z-scored ΔF/F was averaged across trials for each trial type, and then smoothed with a 500-ms boxcar filter (step size 50 ms). The trial-averaged traces in Miss trials were not displayed as the number of Miss trials were zero or very small in most of the cases.

For the analysis in Fig. 2i, we estimated the absolute laminar position (i.e. distance from pial surface) of each cell by adding its relative mediolateral position in the field of view to 1) the distance between the medial border of the field of view and the medial border of the GRIN

lens (determined by registration with a reference image collected on the 1st day of imaging); and 2) a fixed offset for each animal, corresponding to the distance between the medial border of the lens and the cortical surface, estimated histologically after the imaging experiments. We then plotted the fraction of significant Go-preferring and NG-preferring cells against the laminar position binned at 200 μm.

To quantify the separability between the population activity in Go trials and No-Go trials in Fig. 2j,k, we computed the Euclidean distance for trial-averaged ΔF/F traces of a specified set of cells. In each imaging session, 20 cells were randomly selected, and trial-averaged ΔF/F traces were z-transformed using the entire fluorescence trace. We included both FA and CR trials in the No-Go trials. The Euclidean distance in these 20 cells was then computed for each time point (50 ms resolution) between Go trials and No-Go trials. In each session, the Euclidean distance was normalized by the mean distance during the baseline period. To examine the statistical significance of the Euclidean distance in Fig. 2j, a bootstrapped permutation was performed. We randomly relabeled each trial as Go or No-Go trial and computed the Euclidean distance in each permutation. This was repeated 10,000 times to obtain the null distribution. The P value of the observed Euclidean distance was calculated as the percentile of the null distribution. To test the reliability of the correlation between the animals' performance and log (Euclidean distance) in Fig. 2k, we performed sample-with-replacement from the sessions with 10,000 resamples to obtain the distribution of Pearson's correlation coefficient R. The P value was calculated as the fraction of the resampled $R < 0$ (one-sided test).

For Supplementary Fig. 4, we performed a decoding analysis using pyramidal cell activity measured in the imaging experiments and a correlation coefficient-based classifier[20,55,56]. The activity in each trial (z-scored ΔF/F) was aligned to sample onset, and decoding was performed for each sliding 500 ms bin (step size 100 ms). In each imaging session, we selected 80% of Hit and CR trials as training data and the remaining 20% of each type for testing; all Miss and FA trials were used for testing. The activity templates for Go and No-Go were computed by averaging all the training data in Hit and CR trials, respectively. For decoding, the Pearson's correlation coefficient (CC) was computed between the activity in each test trial and each of the two templates; a test trial was classified as Go/No-Go if the CC was higher/lower for the Hit than for the CR template. We repeated this cross validation procedure 100 times and then computed the proportion of each type of test trials classified as Go.

Electrophysiology data analysis

Task-related activity was examined in each cell by performing a two-way ANOVA with factors of trial types (Go or No-Go trials) and laser (on or off conditions). A cell was deemed a significant "Go-preferring" cell if $P < 0.01$ with higher activity during delay in Go trials than No-Go trials, or as a significant "NG-preferring" cell if $P < 0.01$ with higher activity in No-Go trials. To further analyze the activity, spike trains were smoothed by convolution with a normal Gaussian kernel ($\sigma = 50$ ms) to obtain spike density functions (SDFs).

To examine whether the optogenetic stimulation affected the separability between the population activity in Go and No-Go trials in Supplementary Fig. 7b and Fig. 6c, we computed the Euclidean distance between Go trials and No-Go trials both for laser on and off conditions using trial-averaged SDFs of all the recorded cells (n = 529 cells from 5 VIP-ChR2; n = 226 cells from 6 SST-ChR2 mice). The Euclidean distance was then normalized by the mean distance during the baseline period (1 s period immediately before the start of the sample period) in both conditions. Statistical significance of the difference between laser conditions was determined using bootstrap test. In each round of bootstrapping, the same numbers of cells were re-sampled with replacement and the normalized Euclidean distance was computed on the re-sampled data set. By repeating this procedure 10,000 times, we obtained a distribution of the laser-induced Euclidean distance changes and the confidence intervals. The *P* value of the observed difference was calculated as the fraction of the resampled data < 0 for VIP-ChR2, or > 0 for SST-ChR2 (one-sided test). Statistical significance of the difference between laser conditions was also examined using a bootstrapped permutation. We randomly relabeled each trial as laser-on or laser-off and computed the Euclidean distance in each permutation. This was repeated 10,000 times to obtain the null distribution of the laser-induced Euclidean distance changes. The *P* value of the observed difference was calculated as a percentile of the null distribution.

Behavioral data analysis

For the analysis of behavioral data, correct rate, Hit and FA rates were quantified as follows:

Correct rate = (number of Hits + number of CRs)/total number of trials

Hit rate = number of Hits/(number of Hits + number of Misses)

FA rate = number of FAs/(number of FAs + number of CRs)

Based on the Hit and FA rates, auditory discriminability (d') was quantified by:

$d' = \text{norminv}(\text{Hit rate}) - \text{norminv}(\text{FA rate})$

where norminv is the inverse of the cumulative normal function. Higher d' values indicate better behavioral performance.

Wilcoxon signed-rank test was performed to determine the statistical significance of the behavioral effects caused by optogenetic stimulation.

Randomization

For all optogenetic stimulation experiments, laser stimulation was applied in 50% of pseudo-randomly selected trials, but the same condition never occurred in more than 5 consecutive trials. Both in the delayed Go/No-Go and 2-AFC task, two kinds of auditory stimulus (either 2 kHz or 8 kHz tone) were randomly interleaved, but the same auditory stimulus was never presented more than 5 consecutive times. In the delayed 2-AFC task, the duration of the delay period was chosen randomly from a uniform distribution between 1.5 and 2 s.

Statistics

Statistical analysis was performed using MATLAB. All statistical tests were two-sided unless otherwise stated. No statistical methods were used to pre-determine sample sizes but our sample sizes are similar to those reported in previous publications[27,34]. To assess whether a cell was significantly modulated by the task, one-way ANOVA was used for imaging experiments, and two-way ANOVA was used for electrophysiology experiments. To test whether the fraction of significant Go- and NG-preferring cells changed depending on the distance from pia, one-way ANOVA (5 levels of distance) was used. Wilcoxon signed-rank test was performed to determine the statistical significance of the behavioral effects caused by optogenetic stimulation. The significance of the correlation between the animals' performance and log (Euclidean distance) was tested using a bootstrap test (one-sided test). Statistical significance of the difference in the the Euclidean distance between laser conditions was determined using a bootstrap test (one-sided test) and a bootstrapped permutation test.

Supplementary Material

Refer to Web version on PubMed Central for supplementary material.

Acknowledgments

We thank L. Pinto for the help with setting up the endoscope imaging system, M. Zhang and N. Perwez for technical assistance, University of North Carolina Virus Core and Penn Vector Core for supplying AAV, and V. Jayaraman, R.A. Kerr, D.S., Kim, L.L. Looger, and K. Svoboda from the GENIE Project for providing GCaMP6f. This work was supported by the Uehara Memorial Foundation (T.K.), the Human Frontier Science Program (T.K.), NIH R01 EY018861 (Y.D.) and Howard Hughes Medical Institute (Y.D.).

References

1. Baddeley, AD. Working memory. Clarendon Press; Oxford University Press; 1986.
2. Fuster, JM. The prefrontal cortex. Academic Press/Elsevier; 2008.
3. Miller EK, Cohen JD. An integrative theory of prefrontal cortex function. Annual review of neuroscience. 2001; 24:167–202.
4. Bauer RH, Fuster JM. Delayed-matching and delayed-response deficit from cooling dorsolateral prefrontal cortex in monkeys. Journal of comparative and physiological psychology. 1976; 90:293–302. [PubMed: 819472]
5. Buckley MJ, et al. Dissociable components of rule-guided behavior depend on distinct medial and prefrontal regions. Science. 2009; 325:52–58. [PubMed: 19574382]
6. Funahashi S, Bruce CJ, Goldman-Rakic PS. Dorsolateral prefrontal lesions and oculomotor delayed-response performance: evidence for mnemonic "scotomas". The Journal of neuroscience. 1993; 13:1479–1497. [PubMed: 8463830]
7. Erlich JC, Bialek M, Brody CD. A cortical substrate for memory-guided orienting in the rat. Neuron. 2011; 72:330–343. [PubMed: 22017991]
8. Kopec CD, Erlich JC, Brunton BW, Deisseroth K, Brody CD. Cortical and Subcortical Contributions to Short-Term Memory for Orienting Movements. Neuron. 2015; 88:367–377. [PubMed: 26439529]
9. Guo ZV, et al. Flow of cortical activity underlying a tactile decision in mice. Neuron. 2014; 81:179–194. [PubMed: 24361077]
10. Li N, Chen TW, Guo ZV, Gerfen CR, Svoboda K. A motor cortex circuit for motor planning and movement. Nature. 2015; 519:51–56. [PubMed: 25731172]

11. Li N, Daie K, Svoboda K, Druckmann S. Robust neuronal dynamics in premotor cortex during motor planning. Nature. 2016; 532:459–464. [PubMed: 27074502]
12. Kim D, et al. Distinct Roles of Parvalbumin- and Somatostatin-Expressing Interneurons in Working Memory. Neuron. 2016; 92:902–915. [PubMed: 27746132]
13. Fuster JM, Alexander GE. Neuron activity related to short-term memory. Science. 1971; 173:652–654. [PubMed: 4998337]
14. Funahashi S, Chafee MV, Goldman-Rakic PS. Prefrontal neuronal activity in rhesus monkeys performing a delayed anti-saccade task. Nature. 1993; 365:753–756. [PubMed: 8413653]
15. Miller EK, Erickson CA, Desimone R. Neural mechanisms of visual working memory in prefrontal cortex of the macaque. The Journal of neuroscience. 1996; 16:5154–5167. [PubMed: 8756444]
16. Romo R, Brody CD, Hernandez A, Lemus L. Neuronal correlates of parametric working memory in the prefrontal cortex. Nature. 1999; 399:470–473. [PubMed: 10365959]
17. Mante V, Sussillo D, Shenoy KV, Newsome WT. Context-dependent computation by recurrent dynamics in prefrontal cortex. Nature. 2013; 503:78–84. [PubMed: 24201281]
18. Baeg EH, et al. Dynamics of population code for working memory in the prefrontal cortex. Neuron. 2003; 40:177–188. [PubMed: 14527442]
19. Fujisawa S, Amarasingham A, Harrison MT, Buzsaki G. Behavior-dependent short-term assembly dynamics in the medial prefrontal cortex. Nature neuroscience. 2008; 11:823–833. [PubMed: 18516033]
20. Liu D, et al. Medial prefrontal activity during delay period contributes to learning of a working memory task. Science. 2014; 346:458–463. [PubMed: 25342800]
21. Courtin J, et al. Prefrontal parvalbumin interneurons shape neuronal activity to drive fear expression. Nature. 2014; 505:92–96. [PubMed: 24256726]
22. Fu Y, et al. A cortical circuit for gain control by behavioral state. Cell. 2014; 156:1139–1152. [PubMed: 24630718]
23. Kim H, Ahrlund-Richter S, Wang X, Deisseroth K, Carlen M. Prefrontal Parvalbumin Neurons in Control of Attention. Cell. 2016; 164:208–218. [PubMed: 26771492]
24. Kvitsiani D, et al. Distinct behavioural and network correlates of two interneuron types in prefrontal cortex. Nature. 2013; 498:363–366. [PubMed: 23708967]
25. Lee S, Kruglikov I, Huang ZJ, Fishell G, Rudy B. A disinhibitory circuit mediates motor integration in the somatosensory cortex. Nature neuroscience. 2013; 16:1662–1670. [PubMed: 24097044]
26. Pi HJ, et al. Cortical interneurons that specialize in disinhibitory control. Nature. 2013; 503:521–524. [PubMed: 24097352]
27. Pinto L, Dan Y. Cell-Type-Specific Activity in Prefrontal Cortex during Goal-Directed Behavior. Neuron. 2015; 87:437–450. [PubMed: 26143660]
28. Sparta DR, et al. Activation of prefrontal cortical parvalbumin interneurons facilitates extinction of reward-seeking behavior. The Journal of neuroscience. 2014; 34:3699–3705. [PubMed: 24599468]
29. Lee SH, et al. Activation of specific interneurons improves V1 feature selectivity and visual perception. Nature. 2012; 488:379–383. [PubMed: 22878719]
30. Chen TW, et al. Ultrasensitive fluorescent proteins for imaging neuronal activity. Nature. 2013; 499:295–300. [PubMed: 23868258]
31. Ghosh KK, et al. Miniaturized integration of a fluorescence microscope. Nature methods. 2011; 8:871–878. [PubMed: 21909102]
32. Zagha E, Ge X, McCormick, David A. Competing Neural Ensembles in Motor Cortex Gate Goal-Directed Motor Output. Neuron. 2015; 88:565–577. [PubMed: 26593093]
33. Meyers EM, Qi XL, Constantinidis C. Incorporation of new information into prefrontal cortical activity after learning working memory tasks. Proc Natl Acad Sci U S A. 2012; 109:4651–4656. [PubMed: 22392988]
34. Zhang S, et al. Selective attention. Long-range and local circuits for top-down modulation of visual cortex processing. Science. 2014; 345:660–665. [PubMed: 25104383]

35. Pfeffer CK, Xue M, He M, Huang ZJ, Scanziani M. Inhibition of inhibition in visual cortex: the logic of connections between molecularly distinct interneurons. Nature neuroscience. 2013; 16:1068–1076. [PubMed: 23817549]
36. Aron AR, Poldrack RA. Cortical and subcortical contributions to Stop signal response inhibition: role of the subthalamic nucleus. The Journal of neuroscience. 2006; 26:2424–2433. [PubMed: 16510720]
37. Wong KF, Wang XJ. A recurrent network mechanism of time integration in perceptual decisions. The Journal of neuroscience. 2006; 26:1314–1328. [PubMed: 16436619]
38. Machens CK, Romo R, Brody CD. Flexible control of mutual inhibition: a neural model of two-interval discrimination. Science. 2005; 307:1121–1124. [PubMed: 15718474]
39. Wimmer K, Nykamp DQ, Constantinidis C, Compte A. Bump attractor dynamics in prefrontal cortex explains behavioral precision in spatial working memory. Nature neuroscience. 2014; 17:431–439. [PubMed: 24487232]
40. Harvey CD, Coen P, Tank DW. Choice-specific sequences in parietal cortex during a virtual-navigation decision task. Nature. 2012; 484:62–68. [PubMed: 22419153]
41. Yamamoto J, Suh J, Takeuchi D, Tonegawa S. Successful execution of working memory linked to synchronized high-frequency gamma oscillations. Cell. 2014; 157:845–857. [PubMed: 24768692]
42. Salazar RF, Dotson NM, Bressler SL, Gray CM. Content-specific fronto-parietal synchronization during visual working memory. Science. 2012; 338:1097–1100. [PubMed: 23118014]
43. Miyashita Y, Chang HS. Neuronal correlate of pictorial short-term memory in the primate temporal cortex. Nature. 1988; 331:68–70. [PubMed: 3340148]
44. Euston DR, Gruber AJ, McNaughton BL. The role of medial prefrontal cortex in memory and decision making. Neuron. 2012; 76:1057–1070. [PubMed: 23259943]
45. Liebe S, Hoerzer GM, Logothetis NK, Rainer G. Theta coupling between V4 and prefrontal cortex predicts visual short-term memory performance. Nature neuroscience. 2012; 15:456–462. [PubMed: 22286175]
46. Jones MW, Wilson MA. Theta rhythms coordinate hippocampal-prefrontal interactions in a spatial memory task. PLoS biology. 2005; 3:e402. [PubMed: 16279838]
47. Narayanan NS, Laubach M. Top-down control of motor cortex ensembles by dorsomedial prefrontal cortex. Neuron. 2006; 52:921–931. [PubMed: 17145511]
48. Harris KD, Shepherd GM. The neocortical circuit: themes and variations. Nature neuroscience. 2015; 18:170–181. [PubMed: 25622573]
49. Schmidt R, Leventhal DK, Mallet N, Chen F, Berke JD. Canceling actions involves a race between basal ganglia pathways. Nature neuroscience. 2013; 16:1118–1124. [PubMed: 23852117]
50. Fonseca MS, Murakami M, Mainen ZF. Activation of dorsal raphe serotonergic neurons promotes waiting but is not reinforcing. Curr Biol. 2015; 25:306–315. [PubMed: 25601545]
51. Tsien JZ, et al. Subregion- and cell type-restricted gene knockout in mouse brain. Cell. 1996; 87:1317–1326. [PubMed: 8980237]
52. Ziv Y, et al. Long-term dynamics of CA1 hippocampal place codes. Nature neuroscience. 2013; 16:264–266. [PubMed: 23396101]
53. Ahrens MB, et al. Brain-wide neuronal dynamics during motor adaptation in zebrafish. Nature. 2012; 485:471–477. [PubMed: 22622571]
54. Kerlin AM, Andermann ML, Berezovskii VK, Reid RC. Broadly tuned response properties of diverse inhibitory neuron subtypes in mouse visual cortex. Neuron. 2010; 67:858–871. [PubMed: 20826316]
55. Meyers EM, Freedman DJ, Kreiman G, Miller EK, Poggio T. Dynamic population coding of category information in inferior temporal and prefrontal cortex. Journal of neurophysiology. 2008; 100:1407–1419. [PubMed: 18562555]
56. Stokes MG, et al. Dynamic coding for cognitive control in prefrontal cortex. Neuron. 2013; 78:364–375. [PubMed: 23562541]

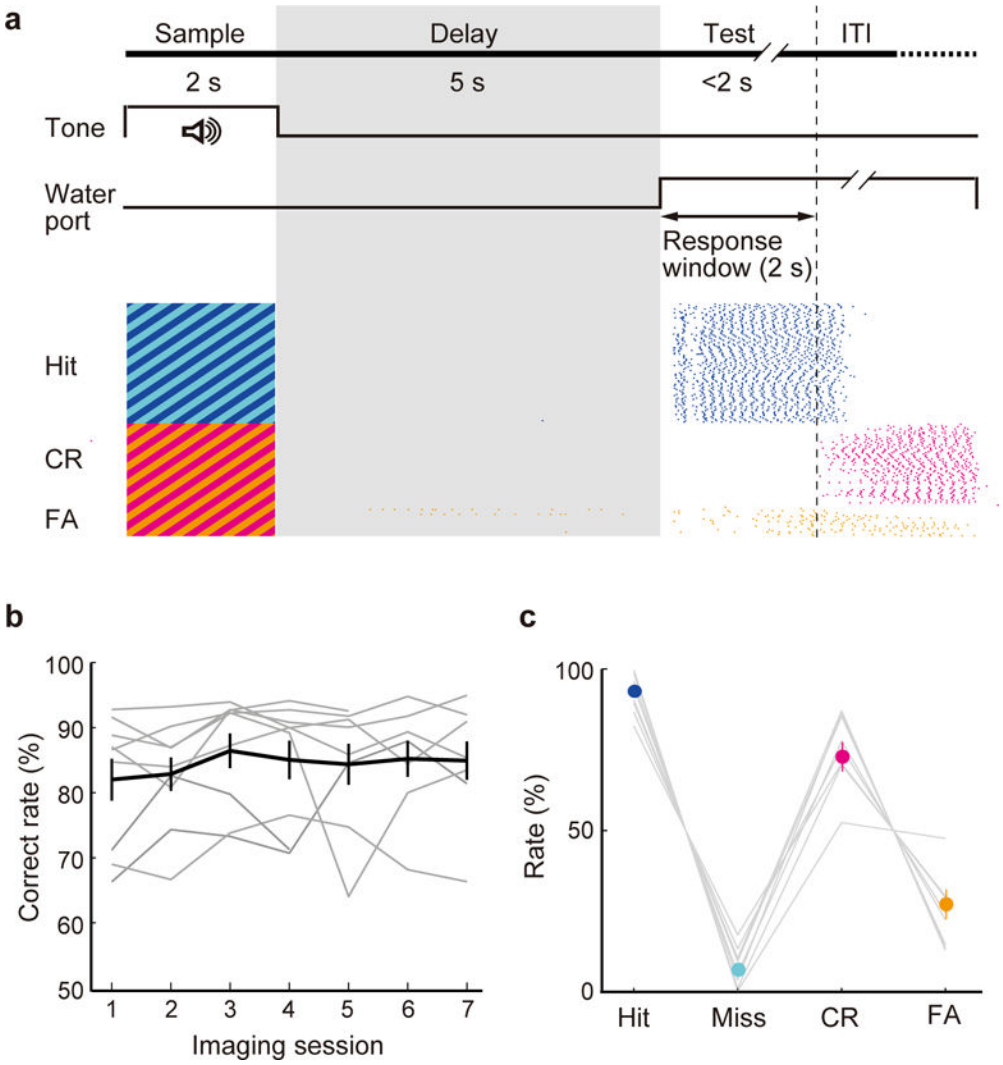

Figure 1. A delayed Go/No-Go auditory task and behavioral performance

(a) Top, schematic for task design. Bottom, licking behavior in an example session. Each tick indicates a lick (blue, Hit; magenta, CR; orange, FA). **(b)** Correct response rates (number of Hit and CR trials divided by the total number of trials) of all CaMKIIα-Cre mice (n = 9) across imaging sessions. Gray lines, individual mice; black, mean ± s.e.m. **(c)** Mean Hit, Miss, CR, and FA rates of all CaMKIIα-Cre mice. Hit + Miss = 100%; CR+FA = 100%.

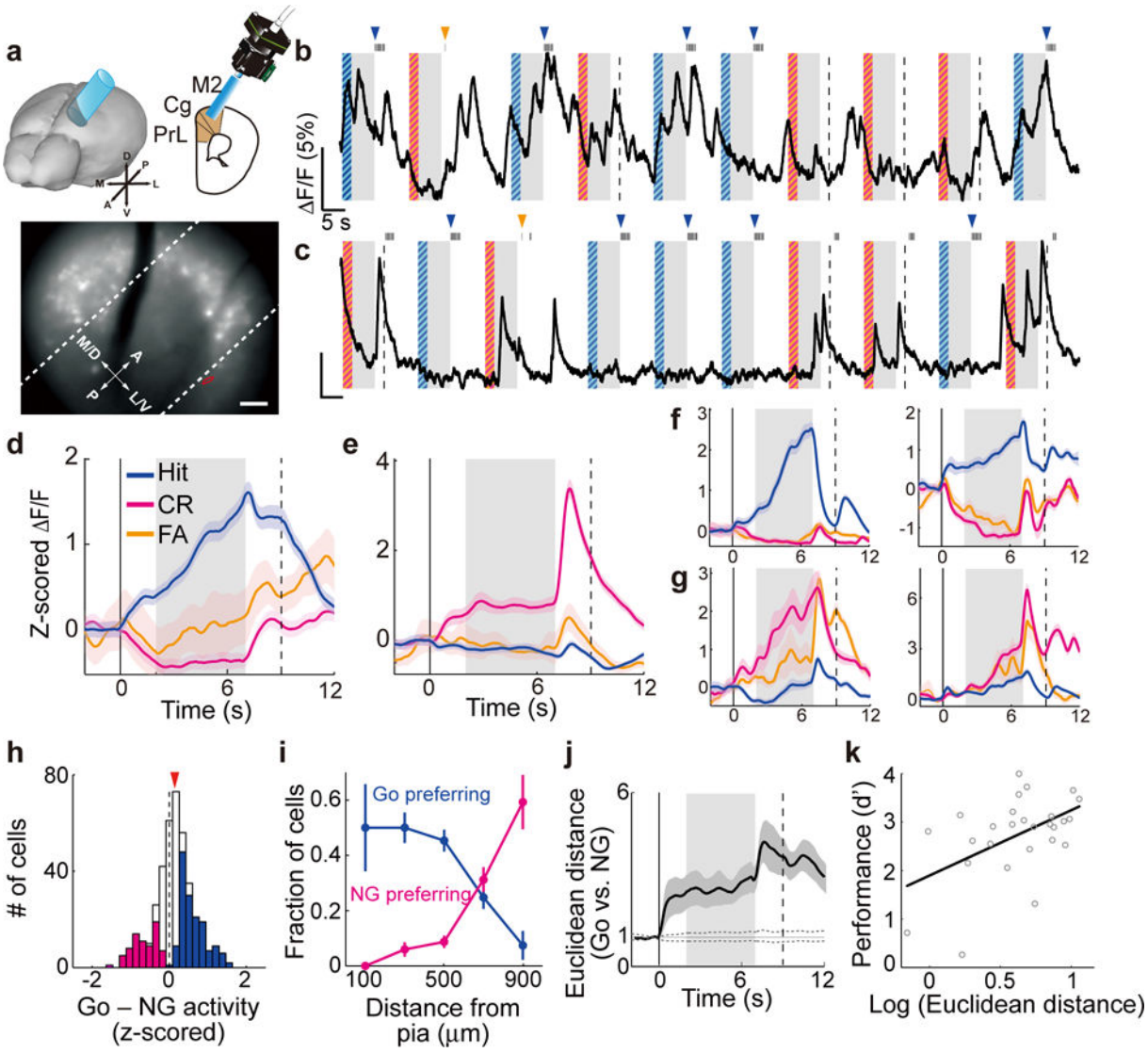

Figure 2. Pyramidal neuron activity during the delayed Go/No-Go task

(a) Schematic of calcium imaging and field of view in an example session. Red outline indicates the example cell shown in (**b**). Dashed lines denote 300 and 600 μm from pia. Scale bar, 100 μm. **(b)** Raw fluorescence trace of the example ROI (outlined in (**a**)). For this cell, the delay activity was larger in Hit than CR trials ($P = 1.5 \times 10^{-24}$, one-way ANOVA). Gray shading, delay period; blue/magenta stripes, sample periods with target/non-target tones. Dashed line, end of response window in CR trials. Black tick on top, lick response. Blue/orange arrowhead, delivery of reward/punishment. **(c)** Same as (**b**), but for a different cell from a different session, delay activity was larger in CR trials ($P = 4.7 \times 10^{-10}$). **(d**,**e)** Trial-averaged ΔF/F (z-scored) of the example ROIs shown in (**b**) and (**c**), respectively. Colored shading, ± s.e.m. **(f**,**g)** Other example significant Go-preferring (**f**) and NG-preferring cells (**g**). **(h)** Distribution of difference in z-scored ΔF/F during the delay period between Go and NG trials in all imaged pyramidal cells (n = 407). Blue/magenta, significant Go-preferring/NG-preferring cells. Red arrowhead, median. **(i)** Fraction of significant Go-

and NG-preferring cells vs. distance from pia. Deep layers had higher fraction of significant NG-preferring cells ($P = 3.7 \times 10^{-14}$, one-way ANOVA). **(j)** Euclidean distance between Go and No-Go activities. Gray dashed trace, 95% confidence interval of shuffled data. **(k)** Behavioral performance (d′) was correlated with the Euclidean distance during the delay period across imaging sessions ($R = 0.50$, $P = 0.0081$, Pearson's correlation coefficient, bootstrap). All colored shadings and error bars, ± s.e.m.

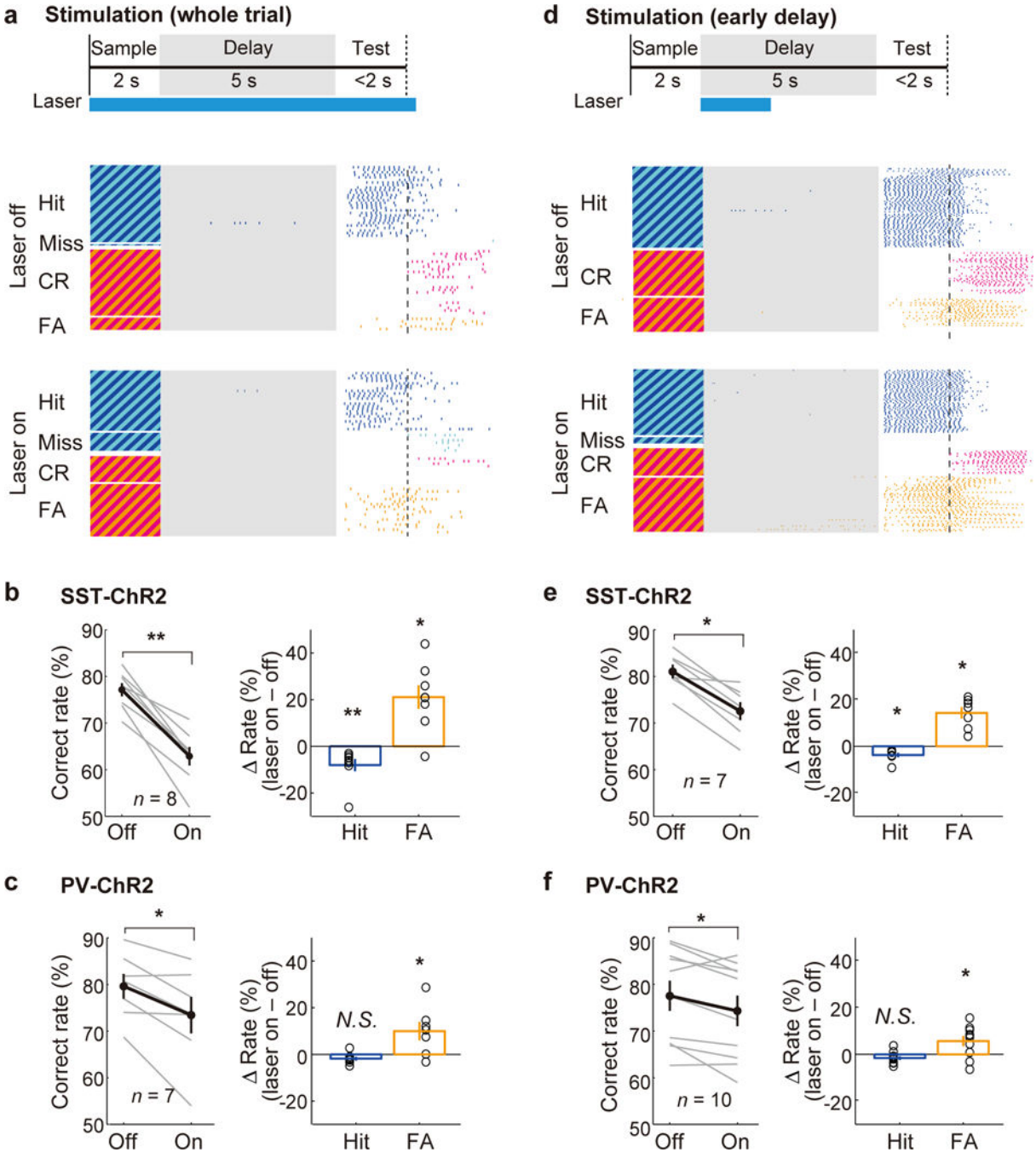

Figure 3. Optogenetic activation of dmPFC SST and PV neurons impaired behavioral performance

(a) Schematic of optogenetic stimulation during the whole trial (top) and an example session of SST neuron stimulation (bottom). Each tick indicates a lick (same as Fig. 1a). **(b)** SST neuron stimulation during the whole trial decreased behavioral performance (n = 8 mice; P = 0.0078, Wilcoxon signed-rank test), with a substantial increase in FA rate (P = 0.016) and a small decrease in Hit rate (P = 0.0078). Gray lines, individual mice; black, mean ± s.e.m. Circles, individual mice. **(c)** PV neuron stimulation also decreased the correct response rate

(n = 7 mice, $P = 0.031$). **(d)** 2-s laser stimulation during the early delay period and an example session of SST neuron stimulation. **(e**,**f)** The early delay stimulation decreased the correct response rate (n = 7 SST-ChR2 mice, $P = 0.016$ (**e**), n = 10 PV-ChR2 mice, $P = 0.027$ (**f**)) with a substantial increase in FA rate. All error bars denote ± s.e.m.

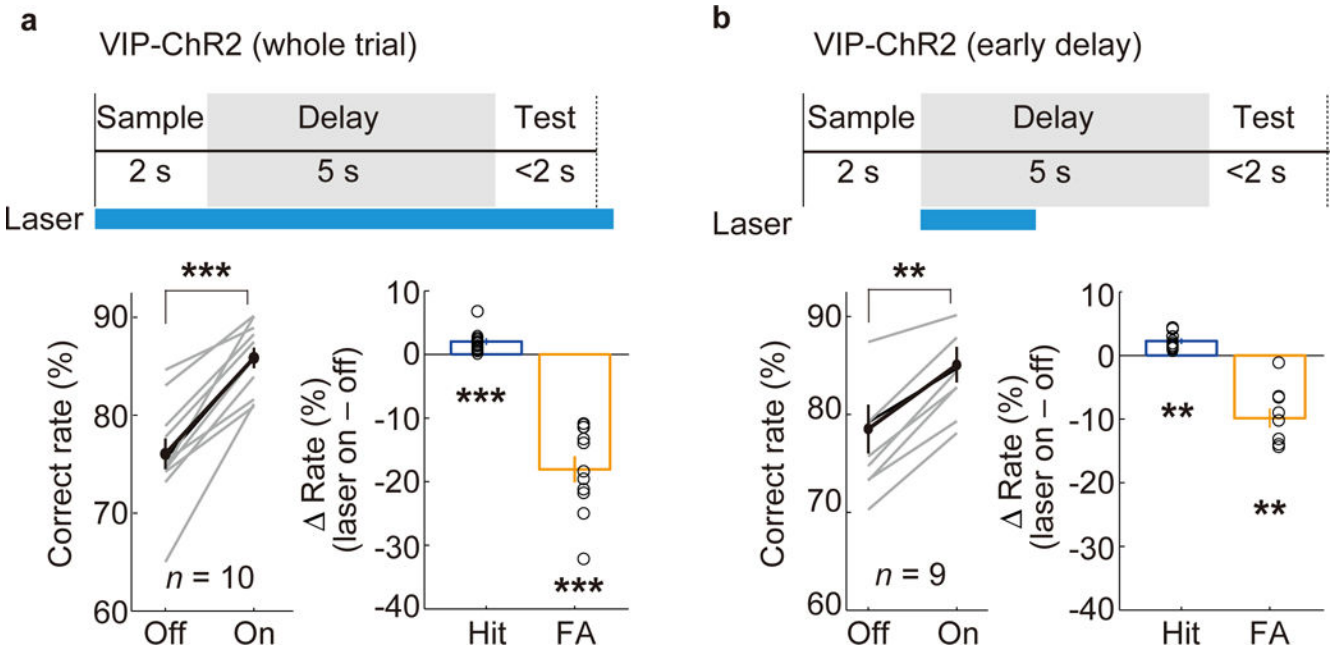

Figure 4. VIP neuron activation improved behavioral performance

(a) Optogenetic activation of VIP neurons during the whole trial increased the correct response rate with a large reduction of FA rate and a small increase in Hit rate (n = 10 mice). **(b)** VIP neuron activation for 2 s during the early delay period also increased the correct response rate (n = 9 mice). All error bars denote ± s.e.m. ** $P = 0.0020$; *** $P = 0.00098$; Wilcoxon signed-rank test.

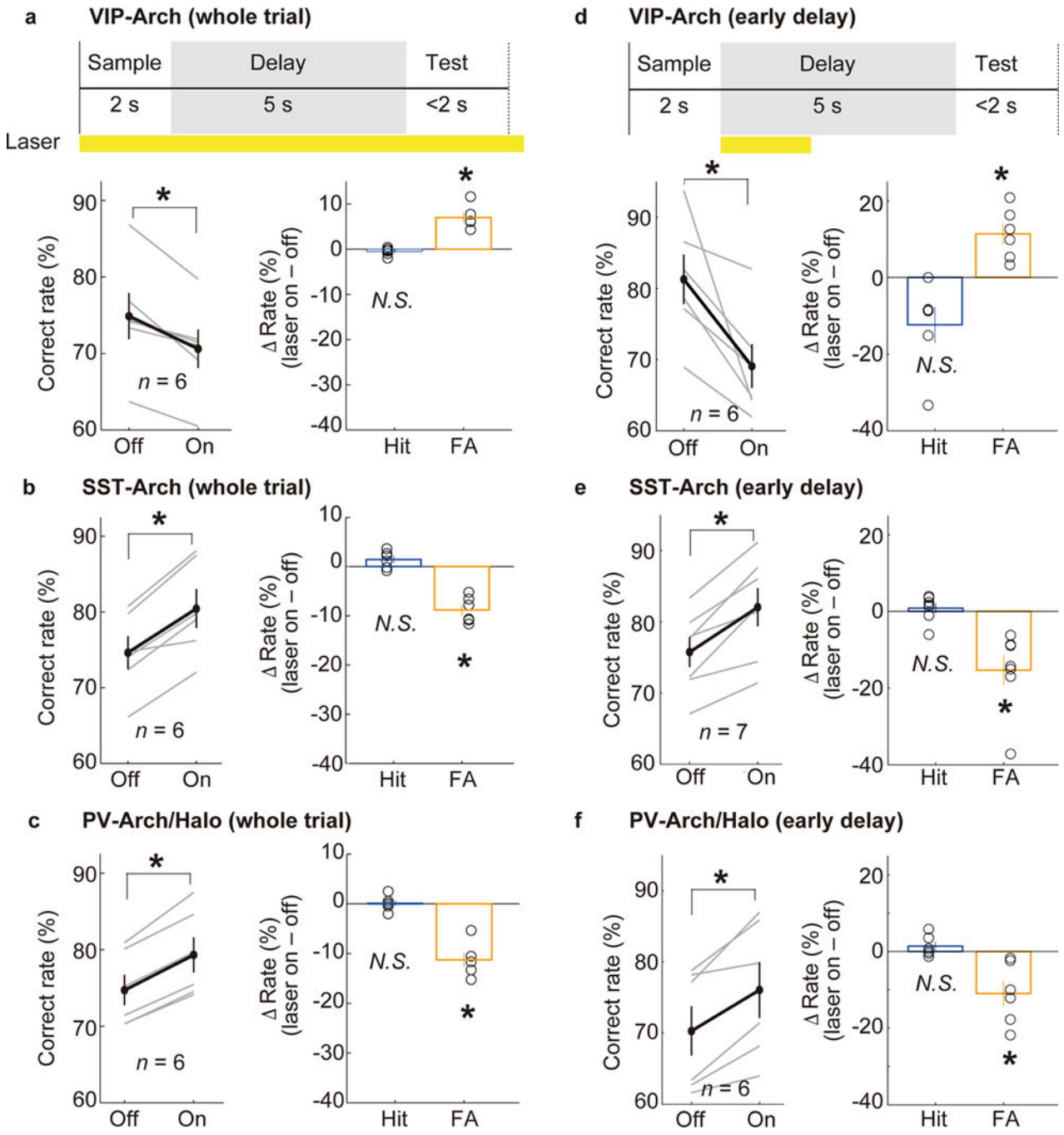

Figure 5. Behavioral effects of optogenetic silencing of VIP, SST, or PV neurons in the dmPFC

(a) Arch-mediated silencing of VIP neurons in the dmPFC during the whole trial decreased the correct response rate ($P = 0.031$, Wilcoxon signed-rank test) due primarily to an increase in the FA rate ($P = 0.031$) rather than the Hit rate ($P = 0.16$). **(b)** Arch-mediated inactivation of SST neurons (whole trial) increased the correct response rate ($P = 0.031$) due primarily to an increase in the FA rate ($P = 0.031$) rather than the Hit rate ($P = 0.16$). **(c)** Arch- or halorhodopsin (Halo)-mediated silencing of PV neurons increased the correct response rate ($P = 0.031$) due primarily to a decrease in FA rate ($P = 0.031$) but not in the Hit rate ($P =$

0.81). **(d–f)** same as **(a–c)**, but silencing during the early delay period. Error bars denote ± s.e.m.

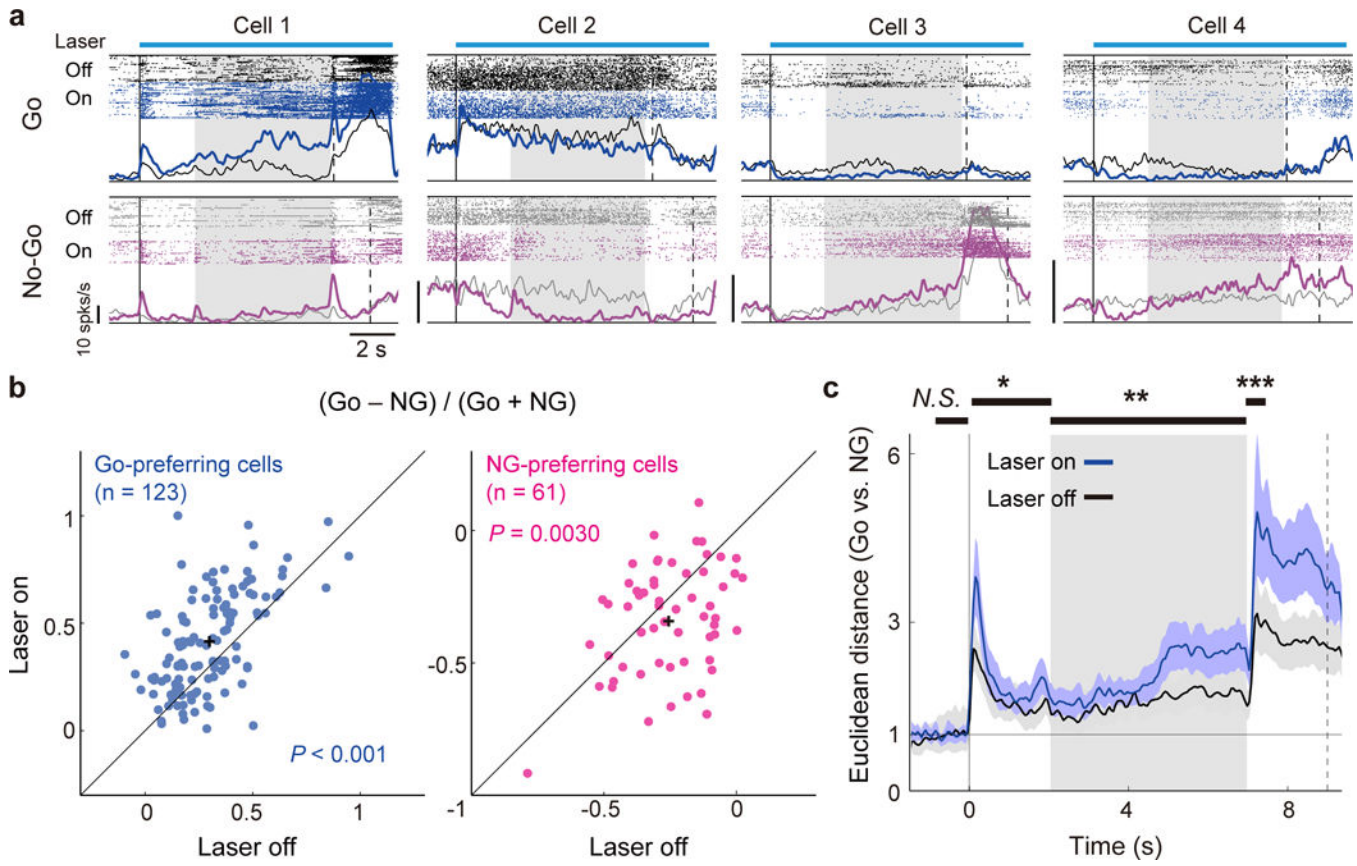

Figure 6. VIP neuron activation improved dmPFC coding of action plan

(a) Spiking activity of example significant Go-preferring (Cells 1 and 2) and NG-preferring cells (Cells 3 and 4) with or without VIP neuron activation. **(b)** Difference between Go and No-Go activity during the delay period in laser on vs. laser off trials, for significant Go-preferring (blue) and NG-preferring (magenta) neurons. The difference divided by their sum increased in Go-preferring cells ($P = 1.1 \times 10^{-9}$, paired t-test) and decreased in NG-preferring cells ($P = 0.0030$) with VIP neuron activation. **(c)** VIP neuron activation increased the Euclidean distance between Go and No-Go activities. The black horizontal bars on the top indicate the analysis periods including baseline (1 s before the beginning of sample), sample, delay, and post-delay (0.5 s after the end of delay) periods. The difference in the Euclidean distance was significant for all analysis periods except for the baseline period ($P = 0.49$; bootstrap). *$P = 0.0060$; **$P = 0.0002$; ***$P = 0$ (bootstrap); Shading and error bars, 95% confidence intervals (bootstrap).

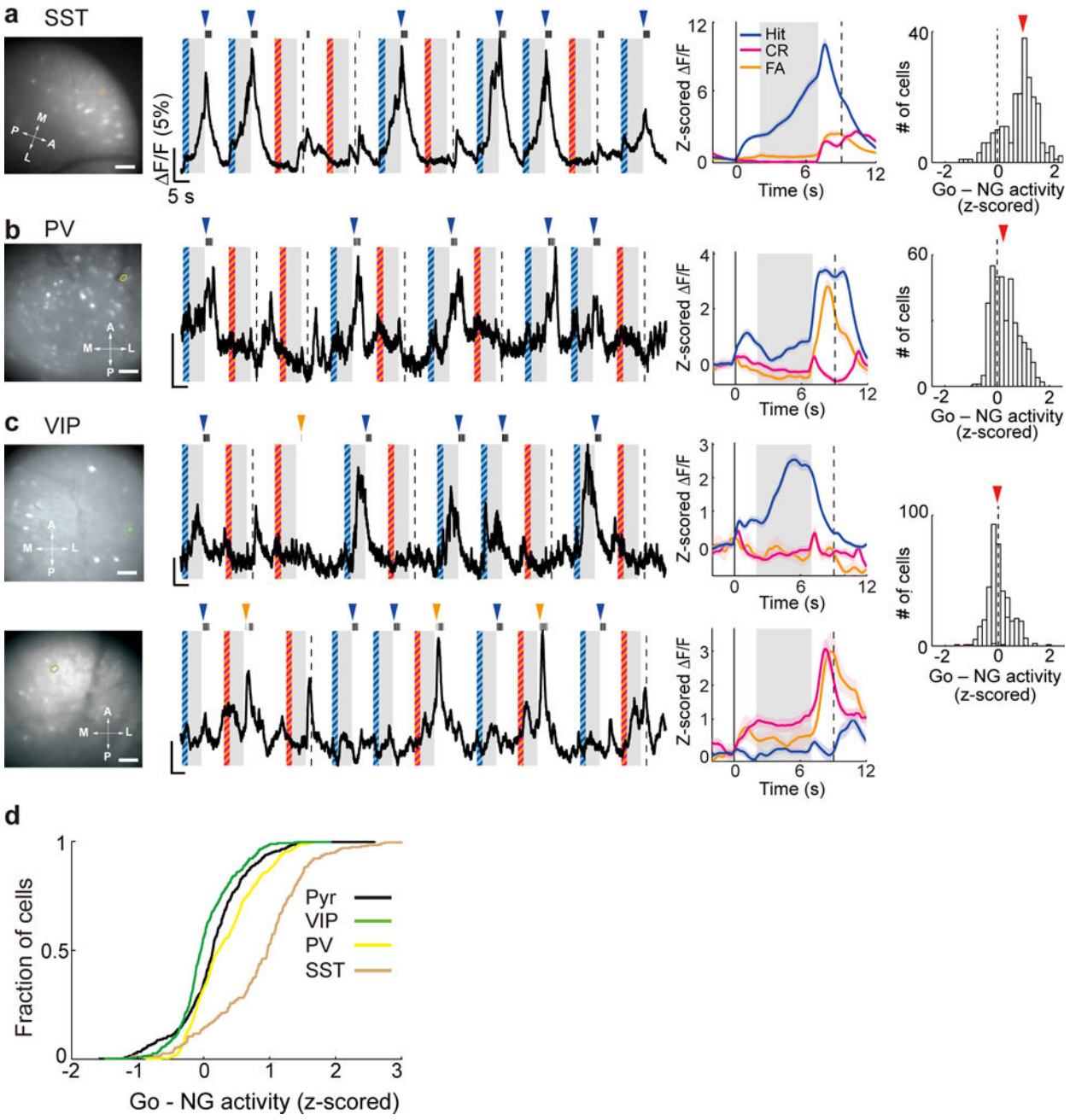

Figure 7. Calcium imaging from each interneuron subtype

(a) Left, Field of view in an example imaging session of SST cells. Brown outline indicates the example ROI shown in the middle panels; Middle, raw fluorescence trace and trial-averaged ΔF/F (z-scored) of the example ROI. The format is the same as Fig. 2b. Right, distribution of Go-NG preference during the delay period in all SST cells (n = 230). Scale bar, 100 μm. **(b)** Same as (**a**) but for PV cells (n = 387). **(c)** Same as (**a**) but for VIP cells (n = 406). The upper and lower panels show two example ROIs with significant Go- and NG-preferring activity, respectively. **(d)** Cumulative distribution of Go-NG preference in the three interneuron subtypes and pyramidal cells (Pyr).

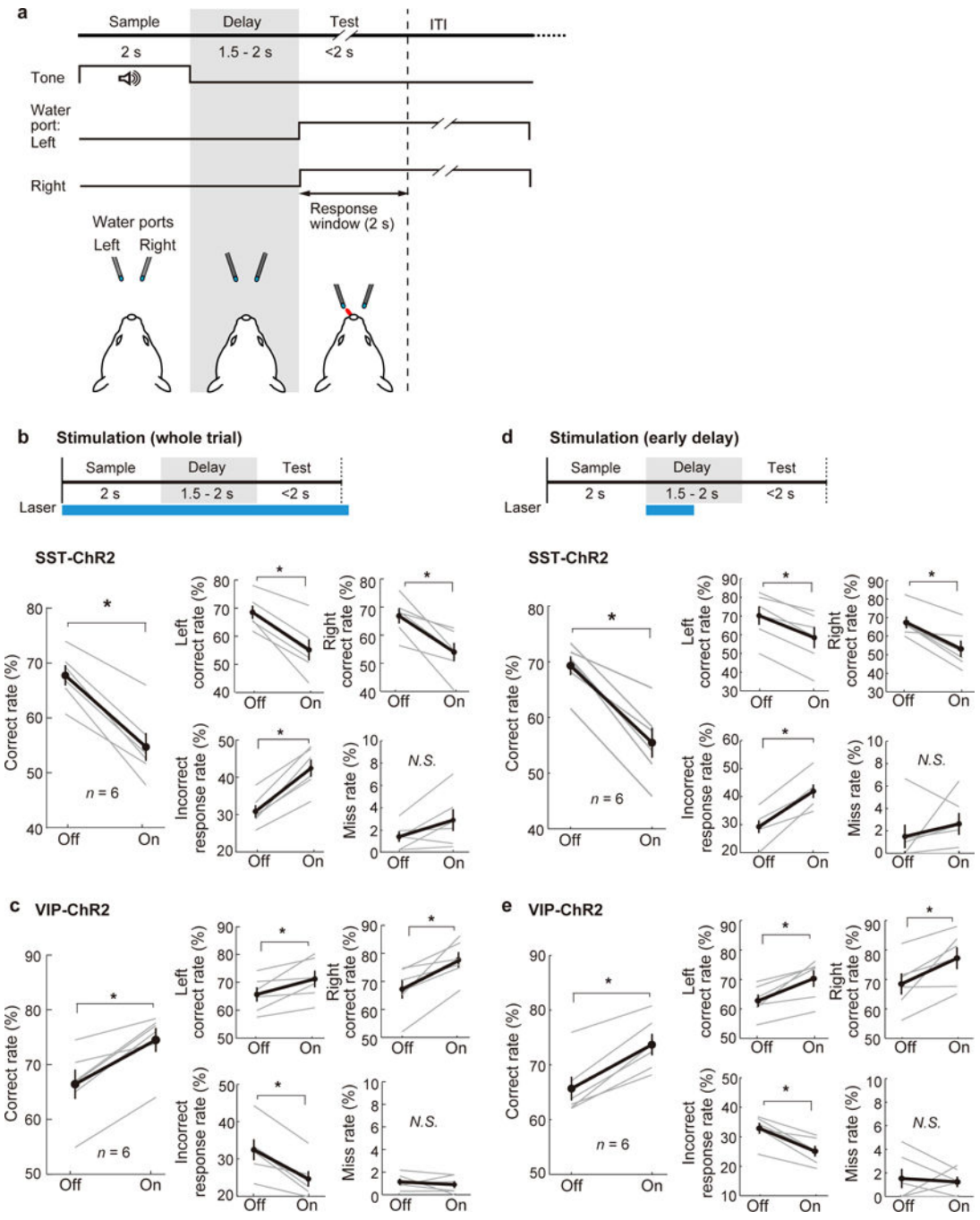

Figure 8. Optogenetic activation of SST and VIP neurons during a delayed two-alternative forced choice (2-AFC) task

(a) Schematic for task design. **(b)** Schematic of optogenetic stimulation during the whole trial (top) and behavioral performance (bottom). Bilateral SST neuron stimulation during the whole trial decreased the correct rate (number of trials with correct responses divided by the total number of trials for each side) in both left and right trials, and increased the incorrect response rate but not the miss rate (n = 6 mice). **(c)** Bilateral VIP neuron stimulation during the whole trial increased the correct rate in both left and right trials, and decreased the

incorrect response rate but not the miss rate (n = 6 mice). **(d,e)** Same as (**b,c**), but with 1-s laser stimulation during the early delay period. Gray lines, individual mice; black, mean ± s.e.m. *P = 0.031; Wilcoxon signed-rank test.